



OPEN

# In-situ and tunable nitrogen-doping of MoS<sub>2</sub> nanosheets

CONFERENCE  
PROCEEDINGS

ACSMS2014

.....

Si Qin, Weiwei Lei, Dan Liu &amp; Ying Chen

Institute for Frontier Materials, Deakin University, Waurn Ponds, Victoria 3216, Australia.

SUBJECT AREAS:

TWO-DIMENSIONAL  
MATERIALS  
SYNTHESIS AND PROCESSING

Molybdenum disulfide (MoS<sub>2</sub>) nanosheets have unique physical and chemical properties, which make it a perfect candidate for next generation electronic and energy storage applications. Herein, we show the successful synthesis of nitrogen-doped MoS<sub>2</sub> nanosheets by a simple, effective and large-scale approach. MoS<sub>2</sub> nanosheets synthesised by this method show a porous structure formed by curled and overlapped nanosheets with well-defined edges. Analysis of the nanosheets shows that they have an enlarged interlayer distance and high specific surface area. X-ray photoelectron spectroscopy analysis shows the nanosheets have Mo-N bond indicating successful nitrogen doping. The nitrogen content of the product can be modulated by adjusting the ratio of starting materials easily within the range from ca. 5.8 to 7.6 at%.

Received  
1 September 2014Accepted  
14 November 2014Published  
23 December 2014

Correspondence and requests for materials should be addressed to W.L. (weiwei.lei@deakin.edu.au) or Y.C. (ian.chen@deakin.edu.au)

Two-dimensional (2D) nanomaterials have distinct properties owing to their extremely small size in one dimension. The common feature of 2D nanomaterials is that they usually contain only one or a few atomic layers. The van der Waals interactions are the dominant force between adjacent layers while much stronger covalent bonding links the atoms with each other within planes. 2D molybdenum disulfide (MoS<sub>2</sub>) has attracted considerable amount of interest in recent years because of its unique properties such as direct bandgap<sup>1,2</sup>, high electron mobility<sup>3</sup>, stable chemical properties and its graphene-like honeycomb lattice.

Different methods have been designed and developed to prepare single and few layers 2D MoS<sub>2</sub> nanomaterials. For the example, the top-down methods, which mainly rely on the exfoliation of layered bulk crystals, include the mechanical exfoliation<sup>4-6</sup>, liquid exfoliation<sup>7</sup>, chemical intercalation and exfoliation<sup>8,9</sup>. On the other hand, there are also bottom-up approaches for synthesizing MoS<sub>2</sub> nanosheets such as chemical vapour deposition (CVD)<sup>10-12</sup>, sol-gel method<sup>13-15</sup> and hydrothermal method<sup>16,17</sup>. However, none of these methods has been reported to be capable of incorporating N content into MoS<sub>2</sub> nanosheets especially in a controllable manner.

Doping can dramatically tune the chemical and physical properties of materials, and has been an essential approach for the functionalising of materials. It has been reported that doping of transition metal can change the electronic properties and enhance the catalytic activity of MoS<sub>2</sub><sup>18,19</sup>. However, the effect of non-metal light elements doping on MoS<sub>2</sub> has yet been widely explored<sup>20</sup>. Some ab initio studies have been carried out to reveal the effect of doping to the electronic properties of MoS<sub>2</sub>, and it has been predicted that doping of non-metal atoms can significantly modify the magnetic and electronic properties of MoS<sub>2</sub><sup>20-23</sup>. Recently, Zhou W. et al reported N self-doped MoS<sub>2</sub> produced by separated nitridation and sulfuration process showing outstanding performance as catalysis for hydrogen evolution reaction<sup>24</sup>. However, it requires complicated and multi-step process and it is unlikely to control the N doping on the final product.

In this paper, we report a different approach for the synthesis of MoS<sub>2</sub> nanosheets with tunable, high concentration and in-situ nitrogen-doping by a simple and cost-efficiency sol-gel process. The synthesised MoS<sub>2</sub> nanosheets have only a few layers and enlarged distance between the adjacent layers. The nitrogen content evaluated by the X-ray photoelectron spectroscopy (XPS) in the nanosheets can be adjusted within the range from 5.8 at% to 7.6 at%. This synthesis approach may open up new paths to non-metal element doping and functionalisation of MoS<sub>2</sub> for other applications such as catalyst and energy storage and conversion devices including lithium ion batteries.

## Results

MoS<sub>2</sub> nanosheets were synthesised using a sol-gel method with molybdenum chloride (MoCl<sub>5</sub>) and thiourea as starting materials. By adjusting the ratio of MoCl<sub>5</sub> and thiourea, we are able to produce MoS<sub>2</sub> nanosheets with almost the same morphology and structure but different N doping level. Products with molar ratio of 1 : 6, 1 : 12 and 1 : 24 will be denoted as MS1-6, MS1-12, and MS1-24 in the following text.

Thermogravimetric analysis (TGA) was performed on the precursor with a starting material ratio of 1 : 6 from room temperature to 1000°C. As shown in Figure 1(a), the weight lost curve can be divided into four parts. The

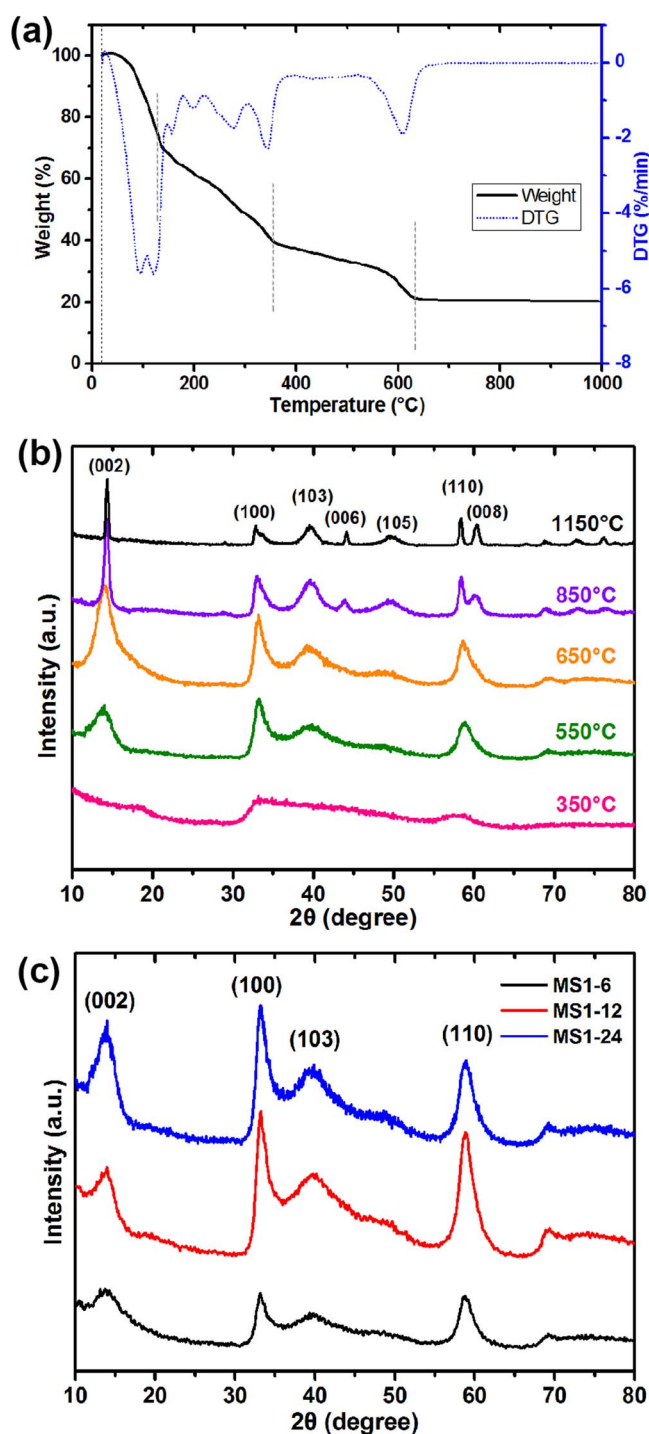


**Figure 1** | TGA and XRD results of the products. (a) TGA result of the precursor of material ratio of 1 : 6 from room temperature to 1000°C. (b) XRD patterns of products of material ratio of 1 : 6 synthesised under different temperature. (c) XRD patterns of products of different material ratio synthesised under 650°C.

first stage of the weight lost began almost right after the heating started. The TGA curve shows a steep weight lost cliff from the room temperature to 130°C, which can be attributed to the evaporation of the remaining ethanol and water in the sample. In the second stage from 130 to 350°C, the starting materials begin to melt and decompose. Thiourea decomposes at a temperature range from 187 to 246°C, releasing various gas including  $\text{NH}_3$ ,  $\text{HNCS}$ ,  $\text{CS}_2$ <sup>25</sup>, leading to 80% of the weight reduction. These gaseous products provide

sulphur to the ensuing reactions, and the gas bubbles also agitate the reaction medium<sup>26</sup>. The third stage shows a gentle slope from 350°C and goes up to 625°C. There is almost no weight lost after the third stage, indicating good thermal stability of the end product of  $\text{MoS}_2$ .

The XRD patterns collected from the products synthesized with a molar ratio of 1 : 6 (MS1-6) under different temperatures are shown in Figure 1(b). The fact that there is no significant diffraction peak in the XRD pattern from the product synthesised at 350°C indicates a disordered and amorphous structure, which suggests that the third stage of the weight lost during the heat treatment described in the TGA curve is crucial in the synthesis, and low temperature annealing is not suitable for the growth of  $\text{MoS}_2$ . The product which synthesised at 550°C has more defined diffraction peaks in the XRD patterns and all the peaks can be indexed as hexagonal  $\text{MoS}_2$  (JCPDS No. 37–1492), but it may still contain some residuals from the starting material according to the TGA result. On the other hand, the product synthesised at 650°C has similar diffraction pattern as the product at 550°C, but the relatively stronger (002) diffraction peak of the product synthesised at 650°C indicates better crystallinity. No signals from impurities can be observed in the XRD patterns. At a higher temperature, diffraction peaks appear sharper and more defined as the temperature rises. The (006) and (008) diffraction peaks only appear at 850°C and above. The appearance of peaks (006) and (008) indicates that the crystal growth is more significant in certain direction under higher temperature, meaning the product becomes bulky and bigger in size. Combine with TGA results above, it suggests that a temperature range between 625°C and 850°C would be suitable for the formation of  $\text{MoS}_2$  nanosheets.

Comparison of the diffraction patterns from the products with different starting material molar ratio synthesised under same temperature of 650°C are shown in Figure 1(c). All the patterns show similarity and negligible difference in aspects of peak position and relative peak intensity. The UV-vis absorption spectra in Supplementary Figure S1(a) show that all the three product exhibit strong UV absorption for wavelength below 320 nm, while bulk  $\text{MoS}_2$  shows no obvious absorption peak. Two absorption peaks observed at around 211 nm and 239 nm could possibly arise from the scattering of the light from the nanosheets<sup>27</sup>. In Supplementary Figure S1(b), we can observe two absorption peaks for bulk  $\text{MoS}_2$  at 634 nm and 692 nm which can be assigned to the excitonic transition characteristic, and a broad peak at around 530 nm which can be assigned to the direct transition from the valence band to the conduction band<sup>27–29</sup>. Similarly, two peaks can be seen from the spectra of the products as well, at around 620 nm and 680 nm. Broad peaks can be seen at around 475 nm, 465 nm and 451 nm for products MS1-6, MS1-12 and MS1-24, respectively. The blue shift of the peaks is possibly due to the quantum confinement of the nanosheets structure<sup>27,30</sup>. The similarity of the three products with different ratio can be not only observed in the XRD results, crystal structure and optical absorption, but also in the morphology revealed by the scanning electron microscopy (SEM) and transmission electron microscopy (TEM) images.

The SEM images of MS1-6, MS1-12 and MS1-24 are shown in Figure 2(a), (c) and (e). One can see the morphology of the three products are quite similar to each other, containing well-defined nanosheets with clear edges. The sponge-like porous framework is formed by the aggregated curl nanosheets with a lot of pores and space between the sheets, which might be created by the gas bubbles from the decomposition of thiourea during the heating process. The TEM images in Figure 2(b), (d) and (f) show overlapped and aggregated nanosheets in all the three products. The images reveal the typical structure of the nanosheets, usually containing 3–8 layers, and the distance between adjacent layers can be estimated from the edge of the sheets. The distance for MS1-6, MS1-12 and MS1-24 were measured to be ca. 0.65 nm, 0.64 nm and 0.64 nm, respectively,

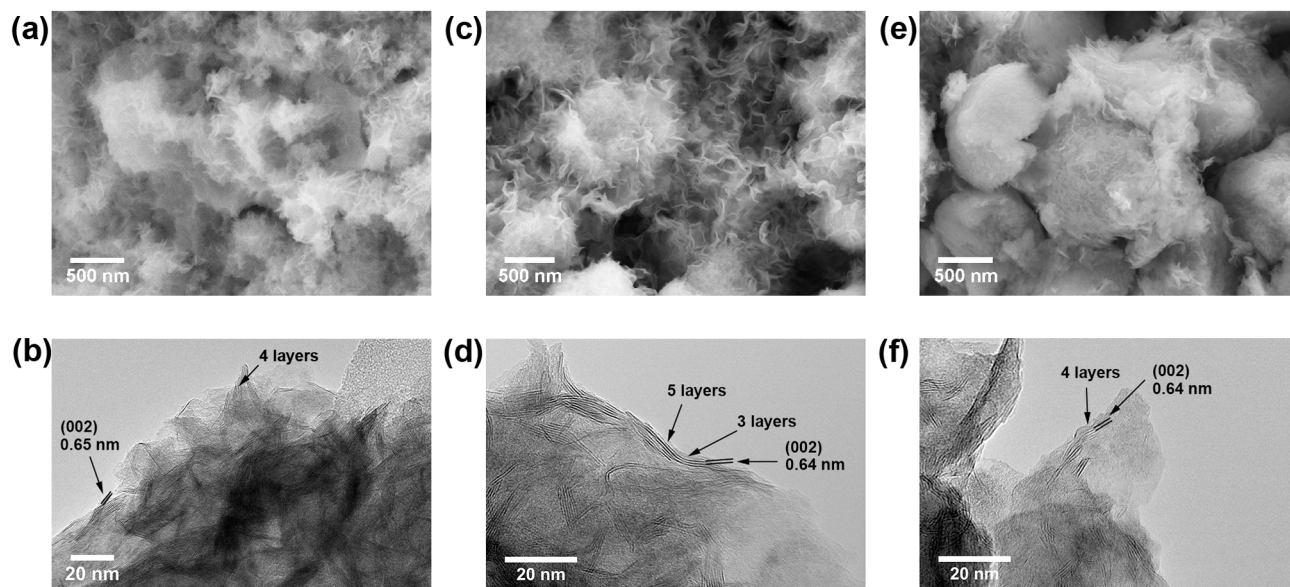


**Figure 2** | SEM and TEM images of the products. SEM images of (a) MS1-6, (c) MS1-12 and (e) MS1-24. TEM images of (b) MS1-6, (d) MS1-12 and (f) MS1-24.

correspond to the (002) planes of hexagonal  $\text{MoS}_2$ . These values are slightly larger than the reported value 0.62 nm for  $\text{MoS}_2$ , which are in accordance with the results of the XRD analysis, suggesting that they have enlarged distance between each layers. Comparing the SEM and TEM images from the three products, it is quite clear that the ratio of thiourea in the precursors does not seem to have a great impact to the final structure and morphology of the nanosheets products.

In order to further understand the formation of the 2D porous structure, nitrogen adsorption-desorption isotherm tests were performed. The results are shown in Figure 3(a), (c) and (e). The isotherms contain typical hysteresis loops in the relative pressure range of 0.4–1.0, indicating a mesoporous structure. Brunauer-Emmett-Teller (BET) calculation reveals that the surface area of products MS1-6, MS1-12 and MS1-24 are  $141.2 \text{ m}^2 \text{ g}^{-1}$ ,  $123.1 \text{ m}^2 \text{ g}^{-1}$ ,

$109.5 \text{ m}^2 \text{ g}^{-1}$ , respectively, arising from the porous structures and the ultrathin dimension of nanosheets. As shown in Figure 3(b), (d) and (f), all the three products have pores with two diameter distributions around 2 nm and 5–20 nm.

XPS spectra were acquired on all three products. As shown in Figure 4(a), there is a hump on the side of  $\text{Mo } 3p_{3/2}$  peak which originates from the N-Mo bond. Curve fitting shows that the overlapped peak locates at 399.2 eV corresponding to N 1s peak from Mo-N bond<sup>24,31</sup>. Another N 1s peak at 402.1 eV can be attributed to the NO adsorbed on the surface of the  $\text{MoS}_2$ <sup>32</sup>. Similarly, the N 1s peaks appear in the spectra for the products MS1-12 and MS1-24 as well. XPS results confirm the substitutional doping of N at the S sites on  $\text{MoS}_2$ . Although the overlap between the  $\text{Mo } 3p_{3/2}$  and N 1s peaks and the shallow analysis depth of XPS method render it difficult to

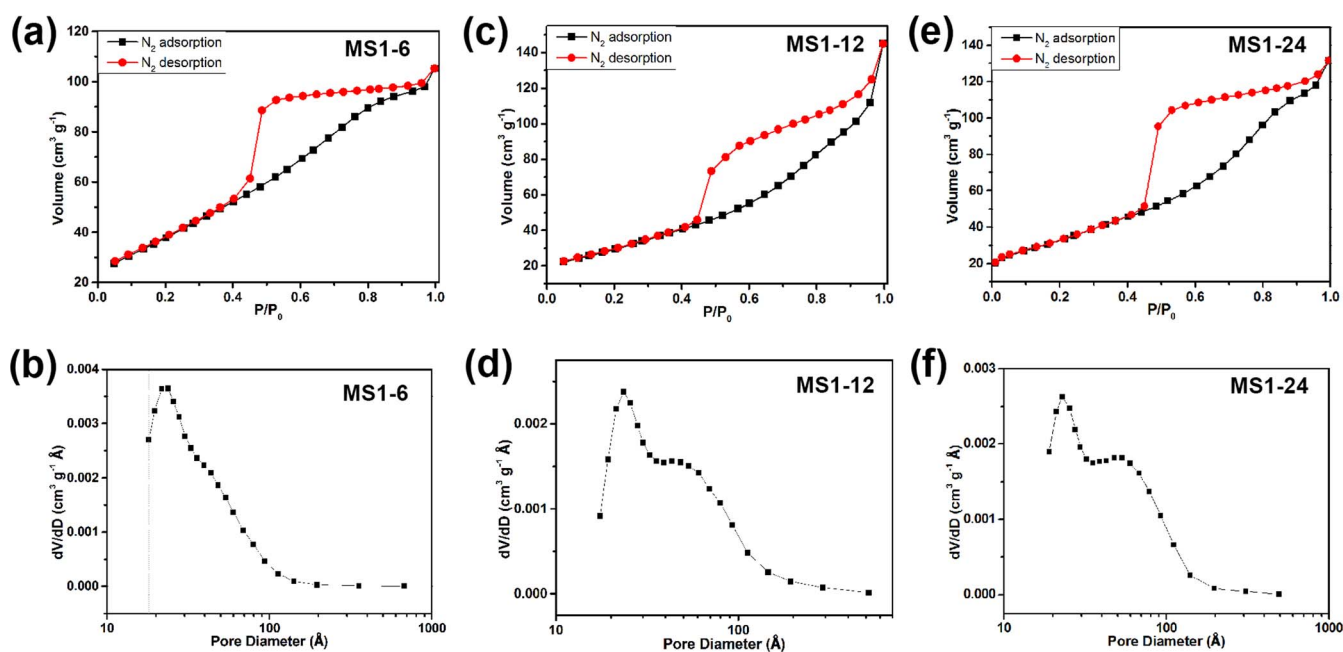


**Figure 3** | Nitrogen adsorption-desorption isotherms of the products. Nitrogen adsorption-desorption isotherm of (a) MS1-6, (c) MS1-12 and (e) MS1-24. Pore size distribution of (b) MS1-6, (d) MS1-12 and (f) MS1-24.

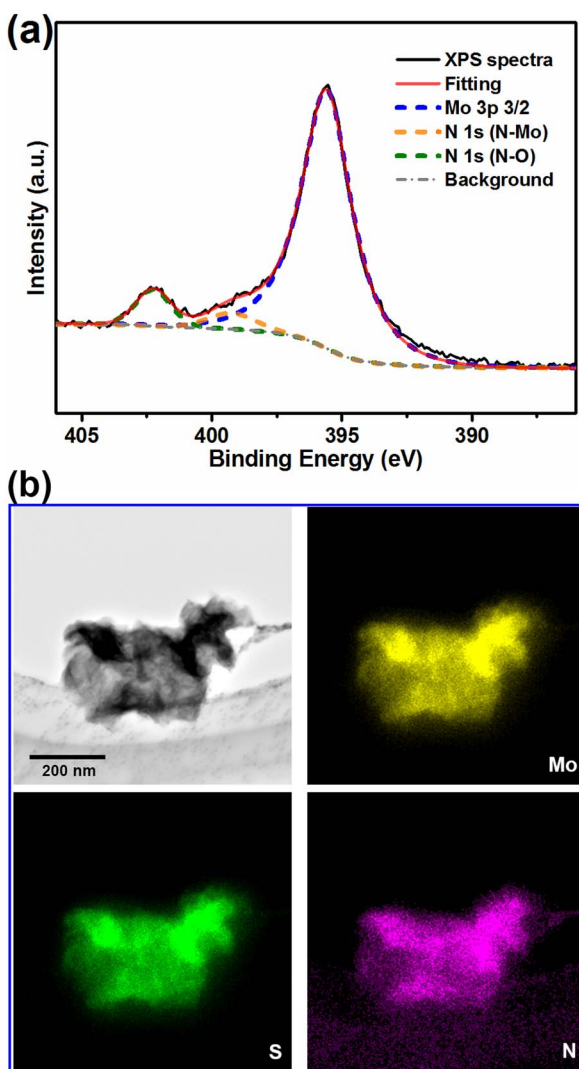


**Figure 4** | XPS and EDS mapping of MS1-6. (a) XPS spectra of the N 1s and Mo 3p region of product MS1-6; (b) TEM image of product MS1-6 and corresponding EDS element mapping of Mo, S and N.

acquire accurate quantitative analysis of the elements, it can still help us to get a qualitative idea of the element composition and understand the N doping effect. As listed in Table 1, analysis of the composition estimates that the products MS1-6, MS1-12 and MS1-24 contain 5.8 at%, 6.4 at% and 7.6 at% of N respectively, excluding the N content from the adsorbed NO. In addition to the XPS results, energy-dispersive X-ray spectroscopy (EDS) mapping were carried out to verify the element distribution. As shown in Figure 4(b), it clearly shows the presence of elements Mo, S and N in the product and the N element was evenly distributed in the nanosheets, which is in agreement with the XPS analysis.

**Table 1** | Concentration of elements Mo, S and N in product MS1-6, MS1-6 and MS1-24, calculated from XPS analysis

Sample	Mo (at %)	S (at %)	N (at %)	BET surface area ( $\text{m}^2\text{g}^{-1}$ )
MS1-6	33.1	61.1	5.8	141
MS1-12	32.8	60.8	6.4	123
MS1-24	33.2	59.3	7.6	110

## Discussion

The above experimental results suggest MoS<sub>2</sub> nanosheets can be successfully synthesised by using a sol-gel method. TGA, XRD and SEM results demonstrate that a temperature around 650 °C is optimized for the formation of MoS<sub>2</sub> nanosheets with a porous structure formed by curled and overlapped nanosheets. The possible formation mechanism of the porous structure can be attributed to the gas bubbles formed during the heating process which act as a sacrificial soft template<sup>26,33</sup>. TEM images and XRD results reveal an enlarged interlayer distance of the nanosheets. The specific surface area of the products evaluated by Nitrogen adsorption and desorption are above 100  $\text{m}^2\text{g}^{-1}$ . Despite the similarity of morphology, crystal structure and porous structure of the three products MS1-6, MS1-12 and MS1-24, the difference in N doping can be revealed by XPS analysis, and the N content can be adjusted from ca. 5.8 to 7.6 at%. EDS mapping shows that the N content is evenly distributed in the MoS<sub>2</sub> nanosheets. Since the N concentration in the final product rises from the starting ratio of thiourea, it can be concluded that it is possible to finely tune the N content in the final product by adjusting the ratio of thiourea without affecting the morphology and the structure of the product.

In summary, we have developed a new simple, efficient and scalable sol-gel approach for the synthesis of MoS<sub>2</sub> nanosheets with controlled N content and large surface area. This approach may open up new paths to non-metal element doping on MoS<sub>2</sub> and finely tune the property and functionalise MoS<sub>2</sub> for other applications, while sol-gel method could be further extended to pave the way to other new 2D nanomaterials with large surface and controlled doping.

## Methods

MoS<sub>2</sub> nanosheets were synthesised using an adapted sol-gel method. In a typical process, about 0.5 g molybdenum chloride (MoCl<sub>5</sub>, Aldrich, 99%) and different molar ratio of (1 : 6 : 1 : 12 and 1 : 24) thiourea ((NH<sub>2</sub>)<sub>2</sub>CS, Alfa-Aesar, 99%), are first mixed in a glass vial. The mixture were dissolved in excessive ethanol in a fume hood by adding ethanol slowly into the vial under stirring, creating a brown solution. The brown gel-like precursor powders were formed after drying and transferred into a quartz boat and heated in a tube furnace for 3 h under 0.1 L  $\text{min}^{-1}$  argon flow at different temperatures, at 350 °C, 550 °C, 650 °C, 850 °C and 1150 °C.

X-ray diffraction (XRD) analysis was performed with a Panalytical X'Pert Powder using Cu K $\alpha$  radiation source with 2 $\theta$  range of 10–80° and a step size of 0.02°. The thermal behaviour of the precursor was analysed using thermogravimetric analysis (TGA) on a Netzsch STA 409 PC/PG thermal analyser at a heating rate of 10 K  $\text{min}^{-1}$  from room temperature to 1000 °C in argon gas flow. UV-vis spectra were collected on a Cary 3 UV-vis spectrophotometer with products dispersed in water. Scanning electron microscopy (SEM) was conducted using a Carl Zeiss Supra instrument. Transmission electron microscopy (TEM) images and energy-dispersive X-ray spectroscopy (EDS) mapping were taken on a JEOL JEM-2100 at an acceleration voltage of 200 kV. Nitrogen adsorption and desorption isotherms were obtained using a Tristar 3000 apparatus at 77 K. X-ray photoelectron spectra (XPS) were acquired on a Kratos AXIS Nova with Al K $\alpha$  X-ray source.

- Mak, K. F., Lee, C., Hone, J., Shan, J. & Heinz, T. F. Atomically Thin MoS<sub>2</sub>: A New Direct-Gap Semiconductor. *Phys. Rev. Lett.* **105**, 136805, doi:10.1103/PhysRevLett.105.136805 (2010).
- Splendiani, A. *et al.* Emerging Photoluminescence in Monolayer MoS<sub>2</sub>. *Nano Lett.* **10**, 1271–1275, doi:10.1021/nl903868w (2010).
- Radisavljevic, B., Radenovic, A., Brivio, J., Giacometti, V. & Kis, A. Single-layer MoS<sub>2</sub> transistors. *Nat Nano* **6**, 147–150, doi:10.1038/nnano.2010.279 (2011).
- Li, H., Wu, J., Yin, Z. & Zhang, H. Preparation and Applications of Mechanically Exfoliated Single-Layer and Multilayer MoS<sub>2</sub> and WSe<sub>2</sub> Nanosheets. *Acc. Chem. Res.* **47**, 1067–1075, doi:10.1021/ar4002312 (2014).
- Chhowalla, M. *et al.* The chemistry of two-dimensional layered transition metal dichalcogenide nanosheets. *Nat Chem* **5**, 263–275, doi:10.1038/nchem.1589 (2013).
- Zhao, Y. *et al.* Interlayer Breathing and Shear Modes in Few-Trilayer MoS<sub>2</sub> and WSe<sub>2</sub>. *Nano Lett.* **13**, 1007–1015, doi:10.1021/nl304169w (2013).
- Coleman, J. N. *et al.* Two-Dimensional Nanosheets Produced by Liquid Exfoliation of Layered Materials. *Science* **331**, 568–571, doi:10.1126/science.1194975 (2011).
- Xiao, J. *et al.* Exfoliated MoS<sub>2</sub> Nanocomposite as an Anode Material for Lithium Ion Batteries. *Chem. Mater.* **22**, 4522–4524, doi:10.1021/cm101254j (2010).
- Zheng, J. *et al.* High yield exfoliation of two-dimensional chalcogenides using sodium naphthalenide. *Nat Commun* **5**, doi:10.1038/ncomms3995 (2014).



10. Lee, W. Y., Besmann, T. M. & Stott, M. W. Preparation of MoS<sub>2</sub> thin films by chemical vapor deposition. *J. Mater. Res.* **9**, 1474–1483, doi:10.1557/JMR.1994.1474 (1994).
11. Lee, Y.-H. *et al.* Synthesis of Large-Area MoS<sub>2</sub> Atomic Layers with Chemical Vapor Deposition. *Adv. Mater.* **24**, 2320–2325, doi:10.1002/adma.201104798 (2012).
12. Yu, Y. *et al.* Controlled Scalable Synthesis of Uniform, High-Quality Monolayer and Few-layer MoS<sub>2</sub> Films. *Sci. Rep.* **3** doi:10.1038/srep01866 (2013).
13. Li, N. *et al.* Preparation of porous MoS<sub>2</sub> via a sol–gel route using (NH<sub>4</sub>)<sub>2</sub>Mo<sub>3</sub>S<sub>13</sub> as precursor. *Mater. Lett.* **88**, 112–115, doi:10.1016/j.matlet.2012.08.031 (2012).
14. Firmiano, E. G. S. *et al.* Graphene oxide as a highly selective substrate to synthesize a layered MoS<sub>2</sub> hybrid electrocatalyst. *Chem. Commun.* **48**, 7687–7689, doi:10.1039/C2CC33397J (2012).
15. Ludi, B., Olliges-Stadler, I., Rossell, M. D. & Niederberger, M. Extension of the benzyl alcohol route to metal sulfides: “nonhydrolytic” thio sol-gel synthesis of ZnS and SnS<sub>2</sub>. *Chem. Commun.* **47**, 5280–5282, doi:10.1039/C1CC10856E (2011).
16. Ramakrishna Matte, H. S. S. *et al.* MoS<sub>2</sub> and WS<sub>2</sub> Analogues of Graphene. *Angew. Chem. Int. Ed.* **49**, 4059–4062, doi:10.1002/anie.201000009 (2010).
17. Chang, K. & Chen, W. Single-layer MoS<sub>2</sub>/graphene dispersed in amorphous carbon: towards high electrochemical performances in rechargeable lithium ion batteries. *J. Mater. Chem.* **21**, 17175–17184, doi:10.1039/C1JM12942B (2011).
18. Cheng, Y. C., Zhu, Z. Y., Mi, W. B., Guo, Z. B. & Schwingenschlöggl, U. Prediction of two-dimensional diluted magnetic semiconductors: Doped monolayer MoS<sub>2</sub> systems. *Phys. Rev. B* **87**, 100401, doi:10.1103/PhysRevB.87.100401 (2013).
19. Zabinski, J. S., Donley, M. S., Walck, S. D., Schneider, T. R. & McDevitt, N. T. The Effects of Dopants on the Chemistry and Tribology of Sputter-Deposited MoS<sub>2</sub> Films. *Tribology Transactions* **38**, 894–904, doi:10.1080/10402009508983486 (1995).
20. Xie, J. *et al.* Controllable Disorder Engineering in Oxygen-Incorporated MoS<sub>2</sub> Ultrathin Nanosheets for Efficient Hydrogen Evolution. *J. Am. Chem. Soc.* **135**, 17881–17888, doi:10.1021/ja408329q (2013).
21. Dolui, K., Rungger, I., Das Pemmaraju, C. & Sanvito, S. Possible doping strategies for MoS<sub>2</sub> monolayers: An ab initio study. *Phys. Rev. B* **88**, 075420, doi:10.1103/PhysRevB.88.075420 (2013).
22. Ataca, C. & Ciraci, S. Functionalization of Single-Layer MoS<sub>2</sub> Honeycomb Structures. *J. Phys. Chem. C* **115**, 13303–13311, doi:10.1021/jp2000442 (2011).
23. Komsa, H.-P. *et al.* Two-Dimensional Transition Metal Dichalcogenides under Electron Irradiation: Defect Production and Doping. *Phys. Rev. Lett.* **109**, 035503 (2012).
24. Zhou, W. *et al.* MoO<sub>2</sub> nanobelts@nitrogen self-doped MoS<sub>2</sub> nanosheets as effective electrocatalysts for hydrogen evolution reaction. *J. Mater. Chem. A* **2**, 11358–11364, doi:10.1039/C4TA01898B (2014).
25. Wang, S., Gao, Q. & Wang, J. Thermodynamic Analysis of Decomposition of Thiourea and Thiourea Oxides. *J. Phys. Chem. B* **109**, 17281–17289, doi:10.1021/jp051620v (2005).
26. Lei, W., Portehault, D., Liu, D., Qin, S. & Chen, Y. Porous boron nitride nanosheets for effective water cleaning. *Nat Commun* **4**, 1777, doi:10.1038/ncomms2818 (2013).
27. Vasic, B. *et al.* Optical properties of exfoliated MoS<sub>2</sub> coaxial nanotubes - analogues of graphene. *Nanoscale Research Letters* **6**, 593, doi:10.1186/1556-276X-6-593 (2011).
28. Butler, S. Z. *et al.* Progress, Challenges, and Opportunities in Two-Dimensional Materials Beyond Graphene. *ACS Nano* **7**, 2898–2926, doi:10.1021/nn400280c (2013).
29. Guardia, L. *et al.* Production of aqueous dispersions of inorganic graphene analogues by exfoliation and stabilization with non-ionic surfactants. *RSC Adv.* **4**, 14115–14127, doi:10.1039/C4RA00212A (2014).
30. Yuwen, L. *et al.* General synthesis of noble metal (Au, Ag, Pd, Pt) nanocrystal modified MoS<sub>2</sub> nanosheets and the enhanced catalytic activity of Pd-MoS<sub>2</sub> for methanol oxidation. *Nanoscale* **6**, 5762–5769, doi:10.1039/C3NR06084E (2014).
31. Inumaru, K., Baba, K. & Yamanaka, S. Preparation of superconducting molybdenum nitride MoN<sub>x</sub> (0.5 ≤ x ≤ 1) films with controlled composition. *Physica B: Condensed Matter* **383**, 84–85, doi:10.1016/j.physb.2006.03.064 (2006).
32. Shuxian, Z., Hall, W. K., Ertl, G. & Knözinger, H. X-ray photoemission study of oxygen and nitric oxide adsorption on MoS<sub>2</sub>. *J. Catal.* **100**, 167–175, doi:10.1016/0021-9517(86)90082-5 (1986).
33. Lei, W. *et al.* Oxygen-doped boron nitride nanosheets with excellent performance in hydrogen storage. *Nano Energy* **6**, 219–224, doi:10.1016/j.nanoen.2014.04.004 (2014).

## Acknowledgments

Financial support from the Australian Research Council Discovery Project, the Australian Research Council Discovery Early Career Researcher Award scheme, and Deakin University, Central Research Grant Scheme are acknowledged. Authors thank Dr Robert Jones from Centre for Materials and Surface Science of La Trobe University for the support in XPS.

## Author contributions

S.Q. and W.L. conceived the project and designed the experiments. S.Q. synthesised the MoS<sub>2</sub> nanosheets and performed the experiments. S.Q., W.L., D.L. and Y.C. contributed to analyses the data and discussions regarding the research. S.Q., W.L. and Y.C. wrote the manuscript.

## Additional information

Supplementary information accompanies this paper at <http://www.nature.com/scientificreports>

**Competing financial interests:** The authors declare no competing financial interests.

**How to cite this article:** Qin, S., Lei, W., Liu, D. & Chen, Y. In-situ and tunable nitrogen-doping of MoS<sub>2</sub> nanosheets. *Sci. Rep.* **4**, 7582; DOI:10.1038/srep07582 (2014).



This work is licensed under a Creative Commons Attribution-NonCommercial-ShareAlike 4.0 International License. The images or other third party material in this article are included in the article's Creative Commons license, unless indicated otherwise in the credit line; if the material is not included under the Creative Commons license, users will need to obtain permission from the license holder in order to reproduce the material. To view a copy of this license, visit <http://creativecommons.org/licenses/by-nc-sa/4.0/>